Elsevier Editorial System(tm) for Water Research
Manuscript Draft

Manuscript Number:

Title: Interrogating chemical variation via layer-by-layer SERS during biofouling and cleaning of nanofiltration membranes with further investigations into cleaning efficiency

Article Type: Research Paper

Keywords: biofouling; biofilm; chemical composition; cleaning efficiency; nanofiltration membrane; surface-enhanced Raman spectroscopy

Corresponding Author: Prof. Kaisong Zhang, PhD

Corresponding Author's Institution: IUE

First Author: Li Cui

Order of Authors: Li Cui; Pengyu Chen; Dayi Zhang; Junyi Li ; Francis L. Martin; Kaisong Zhang, PhD

Abstract: Periodic chemical cleaning is an essential step to maintain nanofiltration (NF) membrane performance and mitigate biofouling, a major impediment in high-quality water reclamation from wastewater effluent. To target the important issue of how to clean and control biofouling more efficiently, this study developed surface-enhanced Raman spectroscopy (SERS) as a layer-by-layer tool to interrogate the chemical variations during both biofouling and cleaning processes. The fact that SERS only reveals information on the surface composition of biofouling directly exposed to cleaning reagents makes it ideal for evaluating cleaning processes and efficiency. SERS features were highly distinct and consistent with different biofouling stages (bacterial adhesion, rapid growth, mature and aged) of biofilm. Cleaning was performed on two levels of biofouling after 18 h (rapid growth of biofilm) and 48 h (aged biofilm) development. An opposing profile of SERS bands between biofouling and cleaning was observed and this suggests a layer-by-layer cleaning mode. In addition, further dynamic biochemical and infrastructural changes were demonstrated to occur in the more severe 48-h biofouling, resulting in the easier removal of sessile cells from the NF membrane. Biofouling substance-dependent cleaning efficiency was also evaluated using the surfactant sodium dodecyl sulfate (SDS). SDS appeared more efficient in cleaning lipid than polysaccharide and DNA. Protein and DNA were the predominant residual substances (irreversible fouling) on NF membrane leading to permanent flux loss. The chemical information revealed by layer-by-layer SERS will lend new insights into the optimization of cleaning reagents and protocols for practical membrane processes.

Suggested Reviewers: Anthony Gordon Fane
SINGAPORE MEMBRANE TECHNOLOGY CENTRE, NTU
AGFane@ntu.edu.sg
expert in membrane fouling, membrane precess and membrane water treatment

Kuolung Tung
Department of Chem Eng. National Taiwan University
kltung@ntu.edu.tw
Expert in fouling, Biofouling and membrane technology

Wei Huang

Dept. of Eng.Sci., University of Oxford
wei.huang@eng.ox.ac.uk
Raman studies of bacteria and biofilm

Sumeet Mahajan
Institute of Life Sciences, University of Southampton
S.Mahajan@soton.ac.uk
SERS studies of cells

Ian Thompson
Dept. of Eng.Sci., University of Oxford
ian.thompson@eng.ox.ac.uk
Expert in water treatment and SERS.

Lab of Membrane Material & Technology
Institute of Urban Environment, Chinese Academy of Sciences
Prof. Dr. Kaisong Zhang
(E-mail:kszhang@iue.ac.cn,Tel/Fax:+86-592 6190782/6190534)
1799 Jimei Road, Xiamen 361021, China http: //www.iue.cas.cn

8 July, 2015

Dear Editor

I would be most grateful if you would consider the uploaded manuscript entitled "**Interrogating chemical variation *via* layer-by-layer SERS during biofouling and cleaning of nanofiltration membranes with further investigations into cleaning efficiency**" for publication in *Water Research*. This original work has been submitted exclusively to this journal. All authors have seen and approved the submitted version of this manuscript.

The understanding of biofouling and the process of eliminating this problem in membranes for water reclamation remains significantly limited. To address how to clean biofouling of nanofiltration membranes for wastewater reclamation more efficiently, we applied surface-enhanced Raman spectroscopy (SERS) as an *in situ* and layer-by-layer tool to interrogate chemical variation of biofouling during both formation and cleaning processes. This approach reveals only the surface composition of biofouling (*i.e.*, the site directly exposed to cleaning) and makes SERS ideal for evaluating the cleaning process and efficiency. It not only allows us to lend new insights into the temporal and spatial composition of biofouling in the form of chemical composition and infrastructure, but also determine the response of the biofouled membrane to a typical cleaning reagent. We believe that this mechanistic analytical tool is potentially translatable to a diverse number of situations, including the industrial workplace. As such, it could significantly improve our treatment of membranes for biofouling. We believe that this will be of significant interest to a wide audience of people working in this area.

The manuscript has been prepared according to the Guide to Authors. We look forward to the Reviewers' positive comments.

Best regards,

Kaisong Zhang

Highlights

- Layer-by-layer *in situ* chemical interrogation of biofouling by SERS
- Opposing alterations in biofouling composition during formation and cleaning
- Chemical infrastructure in 48 h biofouling enhanced cleaning-induced cell removal
- Cleaning is most efficient against lipids than other biofouling compositions
- Irreversible fouling is dominated by DNA and protein biomolecules

Graphical Abstract

Graphical abstract

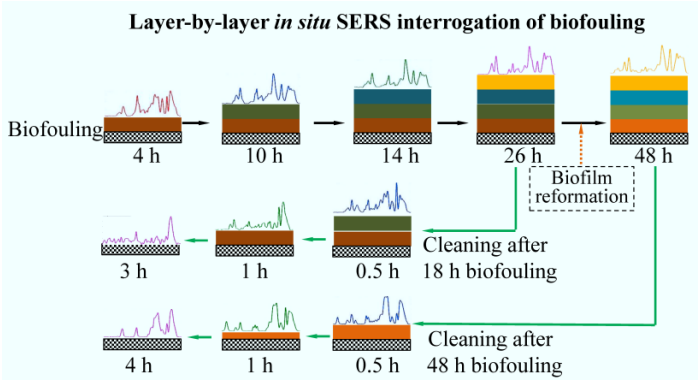

Interrogating chemical variation *via* layer-by-layer SERS during biofouling and cleaning of nanofiltration membranes with further investigations into cleaning efficiency

Li Cui[a,*], Pengyu Chen[a], Dayi Zhang[b], Junyi Li[b], Francis L. Martin[b], Kaisong Zhang[a,*]

[a]Key Laboratory of Urban Pollutant Conversion, Institute of Urban Environment, Chinese Academy of Sciences, Xiamen 361021, China

[b]Centre for Biophotonics, Lancaster Environment Centre, Lancaster University, Lancaster LA1 4YQ, United Kingdom

*Corresponding author.

Tel/fax: +86-592-6190534

E-mail address: lcui@iue.ac.cn (L. Cui), kszhang@iue.ac.cn (K. S. Zhang)

Abstract

Periodic chemical cleaning is an essential step to maintain nanofiltration (NF) membrane performance and mitigate biofouling, a major impediment in high-quality water reclamation from wastewater effluent. To target the important issue of how to clean and control biofouling more efficiently, this study developed surface-enhanced Raman spectroscopy (SERS) as a layer-by-layer tool to interrogate the chemical variations during both biofouling and cleaning processes. The fact that SERS only reveals information on the surface composition of biofouling directly exposed to cleaning reagents makes it ideal for evaluating cleaning processes and efficiency. SERS features were highly distinct and consistent with different biofouling stages (bacterial adhesion, rapid growth, mature and aged) of biofilm. Cleaning was performed on two levels of biofouling after 18 h (rapid growth of biofilm) and 48 h (aged biofilm) development. An opposing profile of SERS bands between biofouling and cleaning was observed and this suggests a layer-by-layer cleaning mode. In addition, further dynamic biochemical and infrastructural changes were demonstrated to occur in the more severe 48-h biofouling, resulting in the easier removal of sessile cells from the NF membrane. Biofouling substance-dependent cleaning efficiency was also evaluated using the surfactant sodium dodecyl sulfate (SDS). SDS appeared more efficient in cleaning lipid than polysaccharide and DNA. Protein and DNA were the predominant residual substances (irreversible fouling) on NF membrane leading to permanent flux loss. The chemical information revealed by layer-by-layer SERS will lend new insights into the optimization of cleaning reagents and protocols for practical membrane processes.

Keywords: biofouling; biofilm; chemical composition; cleaning efficiency; nanofiltration membrane; surface-enhanced Raman spectroscopy

1. Introduction

Water scarcity and strict regulations for the disposal of secondary wastewater effluent generates an urgent need for reclamation of this resource, especially in industrial processes requiring high consumption and wastewater generation (Bes-Pia et al., 2010). Nanofiltration (NF) has been widely utilized as a technology for high-quality water reclamation from wastewater effluent in industries, such as textiles, pulp and paper mill (Bes-Pia et al., 2010, Gonder et al., 2011, Judd and Jefferson, 2003). However, fouling is a major impediment in wastewater reclamation. Fouling causes a decline in permeate flux, requires frequent chemical cleaning, shortens membrane lifespan, and therefore significantly increases the operational cost of NF membrane plants (Guo et al., 2012).

The major types of membrane fouling include scaling (Zhang et al., 2012a), organic matter (Liu et al., 2012, Yao et al., 2010), colloidal (Tung et al., 2012) and biofouling (Al-Juboori and Yusaf, 2012, Baek et al., 2011, Chen et al., 2015, Sim et al., 2013, Zhang et al., 2012b). Amongst these, biofouling, caused by undesired microbial attachment and subsequent bioflim development onto the membrane surface, is the most prevalent and problematic fouling type (Flemming, 2002). Biofouling easily occurs, but is hard to eradicate, because bacteria are ubiquitous in wastewater effluent and tiny amounts of initial bacterial contamination on membranes can form a mature biofilm. Additionally, relative abundance of nutrients on membrane surfaces rather than bulk feed and the convective permeate flow also facilitates biofilm growth (Flemming et al., 1997). The typical biofouling (biofilm) structure is a microbial community with bacteria embedded into the self-produced matrix of extracellular polymeric substances (EPS). EPS are biopolymer mixtures mainly composed of protein, nucleic acids, polysaccharide and lipid, and account for 90% of the dry mass

in most biofilms (Flemming and Wingender, 2010). EPS not only induce declines in permeate flux by increasing hydraulic resistance to permeate flow (Herzberg and Elimelech, 2007, Herzberg et al., 2009). They also act as a protective barrier to diffusion by retarding the adequate delivery of disinfection and cleaning agents to the embedded microorganisms (Nguyen et al., 2012), thus rendering such membrane cleaning less effective.

Periodic chemical cleaning and disinfection are essential steps in maintaining membrane performance (Li and Elimelech, 2004). Various chemical cleaning reagents, biocides and disinfectants, have been developed to control and reduce biofilm growth (Huang et al., 2009a, Liikanen et al., 2002, Mendret et al., 2009, Nguyen et al., 2012). The large consumption of cleaning reagents and accompanying energy costs impose a large economic burden on the operation of membrane plants. However, biofilm matrix has a complex chemical composition which varies dynamically with many factors such as development stages, nutrient supply, hydraulics and bacterial species (Chao and Zhang, 2012, Flemming and Wingender, 2010, Houari et al., 2010, Ivleva et al., 2010). For instance, more dead cells were observed in a mature and aged reverse osmosis biofouling compared to early stage (Herzberg and Elimelech, 2007). Storage time of biofouled NF membranes was found to affect both the membrane permeability and cleaning efficiency (Houari et al., 2009). Degradation of EPS by extracellular enzymes was reported to occur extensively in biofilms in order to self-supply carbon and energy sources (Flemming and Wingender, 2010). These observations suggest dramatic chemical variations in biofouling during formation and cleaning processes. A deeper understanding of biofouling composition and dynamic changes can greatly benefit the adoption of appropriate cleaning reagents and effective cleaning protocols. Given the fact that cleaning reagents mainly interact with the surface chemicals of

biofouling, a tool capable of layer-by-layer interrogation of chemical composition is therefore required to investigate the cleaning mechanism and biofouling substance-dependent cleaning efficiency.

Confocal laser scanning microscopy (CLSM) is widely used in biofilm studies. CLSM can characterize the three-dimensional structure of biofilm and quantify the biovolume of bacteria and EPS by staining biofilm with different fluorescent probes (Yuan et al., 2015). Nevertheless, because of the complexity of EPS compositions and a broad fluorescence spectrum, CLSM cannot achieve high specificity for structural analysis. Raman spectroscopy provides whole-organism fingerprint information with all related biomolecules (nucleic acids, protein, lipid, polysaccharides and their metabolites) displaying distinct spectral features, and thus has been utilized to study the chemical heterogeneity of biofilms (Andrews et al., 2010, Ivleva et al., 2009, Sandt et al., 2007, Wagner et al., 2009). However, application of Raman spectroscopy for biofouling on NF membrane has two challenges: 1) very weak signal (one Raman photon out of 10^8 incident photons) and thus low detection sensitivity; and, 2) interference of Raman bands from membrane materials. Surface-enhanced Raman spectroscopy (SERS) has been developed for biofilms studies due to its ultra-sensitivity, even down to single molecule levels (Kneipp et al., 2008), relying on significant electromagnetic enhancement of up to 10^6-10^{14} over normal Raman scattering provided by silver and gold nanoparticles (Ag NPs and Au NPs). Raman signals of molecules adsorbed or in close proximity to these NPs can be greatly enhanced. This short-distance enhancement effect of SERS can thus exclude membrane interferences, and more importantly, ensure revelation of chemicals only on the surface layer of biofouling. SERS has been successfully applied to study chemical composition and distribution on mature biofilms (Ivleva et al., 2009, Ivleva

et al., 2010), chemical variation during biofilm formation from initial attachment to mature biofilm (Chao and Zhang, 2012), dynamic evolution of microbial structure during biofilm development on cellulose membranes (Chen et al., 2015), and protein fouling on PVDF membranes (Cui et al., 2011). However, the biofilm cultivation conditions in previous investigations (*i.e.*, under static or flow-cell cultivation and/or on glass slides) were far removed from that of real membrane biofouling on commercial membranes under pressure-driven crossflow filtration. Moreover, only biofilm formation processes were addressed, largely ignoring the key cleaning process. Considering the differences of biofouling chemical composition between formation and cleaning processes, the biofouling variation during the cleaning process requires more attention. Outcomes will contribute to the selection of cost-effective cleaning reagents and protocols.

To target chemical variation of membrane biofouling and the important issue of how to clean biofouling more efficiently, this work developed a crossflow membrane filtration system to simulate wastewater reclamation using commercial DOW NF90 membranes, synthetic wastewater effluent and a model bacterial strain. A layer-by-layer SERS tool was employed to interrogate the chemical variations during both the biofouling and cleaning processes. Biocompatible Au NPs were used for SERS acquisition to eliminate possible artifacts caused by microbial toxicity of Ag NPs (Chao and Zhang, 2012, Cui et al., 2013, Cui et al., 2015, Ivleva et al., 2010). Dynamic chemical and infrastructural changes within biofouled membranes and their effects on cleaning processes were studied. Biofouling substance-dependent cleaning efficiency and the persistent chemicals contributing to the permanent flux loss were also evaluated. These studies are important towards our understanding of the cleaning process and factors affecting cleaning efficiency.

2. Materials and methods

2.1 Synthetic wastewater effluent and model bacterial strain

An enriched synthetic wastewater effluent was used for NF membrane biofouling development in a crossflow filtration system, based on the secondary effluent quality of a wastewater treatment plant with high-rate biological processes (Herzberg and Elimelech, 2007). Its composition included: 341 mg/L sodium citrate, 61 mg/L KH_2PO_4, 42 mg/L $NaHCO_3$, 117 mg/L NaCl, 148 mg/L $MgSO_4 \cdot 7H_2O$, 50 mg/L NH_4Cl and 1:1000 diluted Luria Bertani (LB) broth in deionized water (Herzberg and Elimelech, 2007). LB broth was prepared by adding 10 g tryptone (Oxoid Ltd., England), 5 g yeast extract (Oxoid Ltd., England) and 10 g NaCl into 1 L deionized water. Unless otherwise stated, all chemicals were purchased from Sinopharm Chemical Reagent Co., Ltd, China. LB broth and synthetic wastewater effluent were sterilized at 121°C for 30 min before use.

Brevundimonas diminuta is a gram-negative rod-shaped bacterium belonging to phyla Proteobacteria; it is found in abundance within biofilms in membrane filtration systems (Kwon et al., 2011). After overnight cultivation in LB broth at 37 °C and 180 rpm, *B. diminuta* reached the later exponential phase with a final optical density (OD_{600}) of 1.0 and concentration of 10^9 CFU (colony forming unit)/mL. After centrifugation at 7,000 rpm for 5 min, *B. diminuta* pellets were re-suspended in synthetic wastewater effluent and used as inoculum in the crossflow filtration system.

2.2 NF membrane and crossflow test unit

A commercial Dow FilmTec^{TM} NF90 polyamide thin film composite nanofiltration membrane was used for biofouling experiments and purchased from Ande Membrane Separation Technology & Engineering (Beijing) Co., Ltd, China. NF90 membrane

was cut into pieces approximating 42 cm^2 (9.027×4.572 cm) so as to be mounted into the CF042 crossflow cell (Sterlitech Co., USA), and stored in 1.5% $NaHSO_3$ solution for at least one month to wet the membrane, recover flux and prevent bacterial growth prior to filtration.

A laboratory-scale crossflow filtration system was used for biofouling experiments (Fig. 1). The system comprised of five CF042 crossflow cells (Sterlitech Co., USA) positioned in a cascade configuration. A branch path was designed for each cell. To switch the feed water from membrane cell to branch path, two valves controlling the inlet and outlet of membrane cell, and one valve controlling the branch path were employed. Such a design can effectively facilitate the termination of one or several membrane cells without disturbing the whole filtration system. The active dimensions of the cell were 9.027×4.572×0.230 cm (length×width×height). The wastewater effluent was stored in a double-layer cylindrical feed tank and pumped by a high-pressure pump (Hydra-Cell, Wanner Engineering Inc. USA). By circulating chilled water throughout the outer layer of the feed tank, the operation temperature was kept at approximately 30°C. A back-pressure regulator and a bypass valve allowed the fine control of 0.5 MPa transmembrane pressure and 8 cm/s crossflow velocity. The retentate flow rate was monitored by a floating disk rotameter. The permeate flux from five membrane cells was recorded every 2 h by an electronic scale. Both permeate and retentate flow were recirculated back to the feed tank.

2.3 Biofouling process

Prior to NF membrane insertion and biofouling process, the whole system was thoroughly disinfected and cleaned according to Herzberg (2007). The baseline performance of NF membrane was obtained by filtrating 3.6 L sterile deionized water

189 at the designed pressure and flow velocity above. After reaching a stable flux of 41
190 $L/m^2/h$, the deionized water was replaced by 4.0 L synthetic wastewater effluent (no
191 LB and NH_4Cl), supplemented with an aliquot of 4 mL *B. diminuta* suspension to
192 achieve a final bacterial count of 10^6 CFU/mL. After recirculation in the system for 2
193 h, allowing bacterial adhesion on the NF membrane, the system was replaced with
194 sterile fresh synthetic wastewater effluent to promote biofilm development. Permeate
195 flow was collected and measured every 2 h to monitor flux change. Filtration in each
196 membrane cell was terminated at 4 (F-4), 10 (F-10), 14 (F-14), 26 (F-26), 48 (F-48)
197 hours, respectively, by switching the feed flow from the membrane cell to branch path.
198 NF membrane was then taken out, gently rinsed by sterile deionized water to remove
199 suspended bacteria, and finally kept at 4°C before analysis.

200 ### *2.4 Cleaning process and cleaning efficiency calculation*

201 After 18 h and 48 h biofouling development, synthetic wastewater effluent was
202 discharged and replaced with 0.025% sodium dodecyl sulfate (SDS) at pH 12.0.
203 Cleaning was performed by recirculating SDS solution at a flow velocity of 48 cm/s
204 without pressure. To maintain a stable cleaning performance, SDS was refreshed
205 every 10 min in the first 30 min, and every 30 min afterwards. The cleaning was
206 terminated by switching the feed flow to branch path, at 0.5 h, 1 h, 3 h for 18 h
207 biofouling (F-18/C-0.5, F-18/C-1 and F-18/C-3), or 0.5 h, 1 h, 4 h for 48 h biofouling
208 (F-48/C-0.5, F-48/C-1 and F-48/C-4), respectively, until the water flux recovery ratio
209 achieved 90%. The cleaning efficiency was evaluated by the water flux recovery ratio
210 between the membrane after cleaning and before cleaning.

2.5 SERS analysis

2.5.1 Au NPs synthesis

Oval-shaped Au NPs (120 nm at long axis) were prepared (Frens, 1973). Briefly, 100 mL of 0.01% (wt/vol) $HAuCl_4$ aqueous solution was heated to boiling under vigorous stirring, followed by the immediate addition of 0.6 mL 1% (wt/vol) trisodium citrate solution, and kept at boiling point for approximately 1 h. The as-prepared Au NPs were proven to be biocompatible, and their SEM image and size distributions have been previously described (Cui et al., 2013, Cui et al., 2015). Au NPs were washed once by ultrapure water (Millipore, USA) and concentrated through centrifugation at 3,000 rpm for 5 min (Eppendorf centrifuge 5430R, Germany). The supernatant was discarded, and the concentrated precipitate was collected for SERS sample preparation.

2.5.2 SERS measurements

The biofouled NF90 membrane wafer (6 mm, diameter) was cut out from the middle of each biofouled membrane (42 cm^2) using a hole puncher. An equal volume of 20 μL concentrated Au NPs was dropped on the surface of the membrane wafer and left to air-dry. SERS spectra were acquired using a LabRAM Aramis (HORIBA Jobin-Yvon) confocal micro-Raman system equipped with a 600 g/mm grating. Excitation was provided by a He-Ne 632.8 nm laser with 70 μW power. A 50× objective (Olympus) with a numerical aperture of 0.55 and a working distance of 8 mm was used to focus the laser beam and collect the Raman signal. To improve the uniformity of SERS signal and minimize possible laser-induced sample damage, DuoScan in the micro-mapping mode with a scanning area of 30×30 μm was used, based on the combination of two mirrors scanning rapidly the laser beam across the

chosen area. Generally, a total of ten SERS spectra were acquired from different randomly chosen areas on each biofouled membrane.

2.5.3 SERS spectral analysis

SERS spectra were pre-processed *via* baseline correction using LabSpec5 software (HORIBA Jobin-Yvon) and wavelet de-noising. Wavelet de-noising, calculation of the means of spectra with standard deviation, and principal component analysis-linear discriminant analysis (PCA-LDA) were performed using the IrootLab toolbox (http://trevisanj.github.io/irootlab/) running on MATLAB 2012a (Martin et al., 2010). PCA-LDA is a combined multivariate analysis technique and was applied to the pre-processed spectra. PCA was used to reduce the spectral variables to about 10-20 factors accounting for >99% of total variance. Subsequent application of LDA, which takes PCA factors as input variables can maximize between-class variance over within-class variance (Martin et al., 2007). Resulting PCA-LDA 2D scores plots reveal the segregation between classes with their similarity or difference being identified on the basis of the distance between clusters (Martin et al., 2010). To visualize the spectral variation within one class (ten individual spectra from one biofouled membrane) or between classes (different biofouled membranes), the class of spectra were moved vertically and depicted by visualizing the mean spectra surrounded by the standard deviation per wavenumber in the form of coronas.

2.6 SEM Analysis

The morphology of biofouled NF membranes before and after cleaning was characterized using a scanning electron microscopy (SEM, Hitachi S-4800, Japan). The samples were initially fixed with 2.5% glutaraldehyde in 0.1 M phosphate buffered saline for 5 h, followed by critical point drying overnight (Auto-Samdri 815

Automatic Critical Point Dryer; Tousimis, Rockville, MD, USA) and gold sputter coating.

3. Results and discussion

3.1 Biofouling process and permeate flux decline

Synthetic wastewater effluent inoculated with *B. diminuta* was used to induce biofouling on NF membranes. Fig. 2 illustrates the average permeate flux of five cascade-connected biofouling experiments terminated at 4, 10, 14, 26 or 48 h respectively. The almost identical pattern of permeate flux decline observed in five cells indicates the reproducibility of the biofouling process (Fig. S1). A slight decline in flux was observed in the first 8 h, probably due to both the concentration polarization of feed solution and deposition of bacteria. Subsequently, a dramatic decline in permeate flux occurred from 8 h to 26 h with the flux decreasing from 85% to 35% of initial levels. Rapid bacterial proliferation and biofilm growth in this stage accounted for this decline, as noted by SEM (Fig. 3). After 26 h, the flux continued to decline, but at a much slower rate, until it reached 27% of initial levels at 48 h. Similar declines in flux were observed by Herzberg (2007) wherein a different bacterium (*P. aeruginosa*) was exploited to induce biofouling on reverse osmosis membranes in a bench-scale crossflow filtration unit.

Biofouling was terminated at five time points representative of different stages of flux decline, *i.e.*, 4 h (slow decline), 10 h (start of rapid decline), 14 h (middle of rapid decline), 26 h (end of rapid decline) and 48 h (slow decline). SEM images (Fig. 3) of surface and cross-sectional views of the five biofouled membranes clearly show biofilm development. Only a sub-monolayer of bacteria was observed on NF membranes at 4 h. Following prolonged filtration time from 10 h to 26 h, biofilm

thickness significantly increased, consistent with the most marked flux decline in this stage. From 26 h to 48 h, thickness increases slowed down, consistent with the slow flux decline, indicating a tailing off of bacterial-cell proliferation likely caused by nutrient depletion (Herzberg and Elimelech, 2007). Meanwhile, gaps between deposited cells as evident in SEM images (surface views) decreased and eventually vanished, indicating EPS production external to biofilm cells induced them to clump together. EPS secretion was most obvious at 48 h, when cells were almost completely embedded inside this matrix. EPS and deposited cells mainly account for flux decline by inducing hydraulic resistance to permeate flow and elevated trans-membrane osmotic pressure (Herzberg and Elimelech, 2007, Herzberg et al., 2009). The slower increase in biofilm thickness from 26 h to 48 h, accompanied with elevated EPS secretion at 48 h, may indicate a transition of biofilm from maturation to aged stage.

3.2 Chemical composition of biofouling during process of formation

Despite the changing course in the flux decline curve and altering biofilm morphology during biofouling development, variations in chemical composition remain obscure, necessitating investigation in order to optimize cleaning reagents and protocols. Therefore, SERS measurements were performed on biofouled NF membranes terminated at the same time as flux monitoring and SEM imaging. Au NPs were dropped on biofouled membranes to provide spectral enhancement. Corresponding SEM images (Fig. 4) indicate that Au NPs completely cover the biofilm with no visible biofilm cells. Additionally, multiple Raman bands arising from NF90 membrane material vanished after Au NP coating (Fig. S2), negating membrane interference. SERS spectra of biofouling are shown in Fig. 5. The narrow corona demonstrates that the spectral variation possibly caused by the heterogeneity of both biofilm and SERS enhancement, was overcome by the combined use of a thick Au

NPs layer and large-area DuoScan mode.

SERS of biofouling generated a large number of peaks, indicating a rich chemical diversity (Fig. 5). Additionally, obvious time-related differences in spectral features indicate a changing chemical signature at different development stages. PCA-LDA was applied to highlight differences in SERS features between biofouled membranes. Each SERS spectrum was plotted as a point in a 2D PCA-LDA scores plot (Fig. 5b), where the segregation distance of each point and cluster was proportional to spectral dissimilarity. Clusters representative of biofouling in exponential phase (10, 14 and 26 h) were more closely aligned, but distinct from lag (4 h) and aged stages (48 h). Therefore, SERS features were consistent in recognizing different development stages of biofouling with the flux decline curve and biofilm morphology.

In comparison, SERS intensity did not markedly change despite the significant increases in biofilm thickness (Fig. 5a), probably due to the short-distance enhancement effect of SERS that only allows molecules adsorbed on or in the very close proximity to Au NPs to be enhanced. Therefore, SERS only reveals the chemical composition of the biofouling surface layer. This makes SERS an appropriate tool for guiding the cleaning of biofouled membranes since only the surface layer of biofouling is directly exposed to cleaning reagents. To understand the chemical origins for the observed alterations of spectral features, SERS band assignment needs to be clarified, which remains a big challenge due to the lack of a comprehensive database of SERS spectra for bacteria or biofilm (Ivleva et al., 2010). This study obtained SERS spectra of various molecules representing typical EPS compositions using Au NPs, namely DNA, protein, polysaccharide and lipid (Fig. S3). Among them, nucleotides and DNA bases represent genomic material; BSA, oligopeptides and phenylalanine represent protein; lipopolysaccharide and

peptidoglycan are typical components of bacterial cell membranes and contain information regarding polysaccharide, protein and lipid; sodium alginate represents polysaccharides; and, lipid was extracted from *B. diminuta*. Referring to SERS spectra of reference molecules and published data, tentative band assignments are given in Table 1, together with Raman intensity changes, *i.e.*, increasing (red arrows) and decreasing (blue arrows), during biofouling and cleaning processes.

Polysaccharides play an important role in bacterial adhesion and retention of water/nutrients (Flemming and Wingender, 2010). Referring to SERS spectra of various polysaccharides including cellulose, dextran, xanthan, gellan and alginic acid, SERS band at 494 cm^{-1} can be found in dextran (Ivleva et al., 2010), as well as lipopolysaccharide and peptidoglycan (Fig. S3). The 550 cm^{-1} band can be observed in dextran. The 1095 and 1126 cm^{-1} bands appear in dextran and cellulose. During biofouling processes, the most obvious changes in polysaccharides were the 494 and 550 cm^{-1} bands, which clearly showed up at 48 h. In comparison, 1095 and 1126 cm^{-1} bands showed small increases at 26 and 48 h. Chao et al. (2012) pointed to increases in polysaccharides from initial bacterial adhesion to mature biofilm, confirming their role in biofilm infrastructure.

DNA, including extracellular DNA (eDNA) and their metabolites, are important for enhancing bacterial adhesion (Andrews et al., 2010) and exchanging genetic information (Flemming and Wingender, 2010). Bands at 737, 1325 cm^{-1} and 660, 1587 cm^{-1} were assigned to adenosine and guanosine-related molecules, respectively, (Fig. S3) (Cui et al., 2013, Cui et al., 2015, Ivleva et al., 2010, Kneipp et al., 2002). Significant increases of all these DNA-related bands were observed at 26 and 48 h, suggesting increases of DNA with larger amounts of EPS secreted in mature and aged biofilm. The results are consistent with previous findings of a higher DNA content in

358 the mature biofilm (Chao and Zhang, 2012). Andrews et al. (2007) also observed a
359 higher Raman intensity of DNA in biofilm cells than planktonic cells.

360 Proteins play unique functions in biofilm development. Various extracellular
361 enzymes are involved in digesting biopolymers to provide carbon and energy sources
362 for biofilm development. Non-enzymatic structural proteins constitute a link between
363 the bacterial surface and EPS to promote matrix stabilization (Flemming and
364 Wingender, 2010). Protein bands in biofouling development processes displayed some
365 changes, with the 1000 cm^{-1} (Phenylalanine) and 1445 cm^{-1} (CH_2 deformation of
366 Protein) (Xu et al., 2014) bands decreasing with time, while 1700 cm^{-1} (Amide I) and
367 1243 cm^{-1} (Amide III) (Huang et al., 2009b) bands increasing, especially at 26 and 48
368 h. Different proteins may be required for biofouling development at different stages.

369 Lipids also exist in EPS matrix and can alter bacterial surface properties in
370 response to varying environmental conditions (Andrews et al., 2010, Ortiz et al., 2009,
371 Pirog et al., 2004). A lipid band (Maquelin et al., 2002) was observed at 1465 cm^{-1}
372 after 10 h biofouling, and kept increasing especially from 26 h to 48 h. The
373 remarkably higher SERS intensity of lipid at 48 h indicates an increasing content in
374 biofilm with EPS secretion than earlier stages, similar to the biofilms formed by
375 gram-negative bacteria (Chao and Zhang, 2012).

376 A carotenoids band at 1533 cm^{-1} (Rosch et al., 2005) was only evident at 4 h but
377 absent subsequently. Andrews et al. (2010) observed carotenoids in planktonic
378 bacteria (*Rhodococcus* and *Sphingomonsa*), but not in their biofilms, indicating that
379 biosynthesis of carotenoids is related to growth conditions and terminates when
380 biofilm is formed. Additionally, 1533 cm^{-1} (carotenoids) and 1445 cm^{-1} (protein) were
381 the two bands exclusively present at 4 h (initial bacterial attachment) but absent
382 subsequently. Considering the short-distance enhancement effect of SERS, the only

explanation for the two missing bands is the lack of interaction of carotenoids and protein with Au NPs by the latterly-formed biofouling layer. This further confirms the ability of SERS to reveal surface composition.

3.3 Chemical composition of biofouling during cleaning process

Cleaning was performed on two levels of biofouling after 18 and 48 h development (F-18 and F-48) in order to investigate chemical composition variation during cleaning and factors affecting this process.

3.3.1 Cleaning after 18 h biofouling

Cleaning efficiency was evaluated by calculating water flux recovery ratio (*i.e.*, the water flux post-cleaning to that of the originally clean membrane), which increased with cleaning time and recovered to 91.2% after 3 h cleaning (F-18/C-3) (Fig. 6). Corresponding SEM images (Fig. 7a) also show an obvious decline in the biofouling thickness with only a sub-monolayer of bacteria remaining on the membrane surface after F-18/C-3.

SERS spectra before and after cleaning are shown in Fig. 8a. Clearly separated clusters in the derived PCA-LDA 2-D scores plot (Fig. 8b) indicate the highly variable spectral features with cleaning. Interestingly, intensities of SERS bands (Table 1) display opposing changes following cleaning *versus* biofouling. Bands at 1095/1126 (polysaccharide), 660 (G), 737 (A), 1325 (A, G), 1700 (protein) and 1465 cm^{-1} (lipid) increased with biofouling, but decreased following cleaning. The phenylalanine band (1000 cm^{-1}) decreased with biofouling, but increased following cleaning. Moreover, the bands at 1533 cm^{-1} (carotenoids) and 1445 cm^{-1} (protein) that only appeared at F-4, showed up again after 0.5 and 1 h cleaning (F-18/C-0.5 and F-18/C-1), further confirming it is the coverage by the latterly-formed fouling layer suggesting their

absence. Such opposing band changes clearly demonstrate the applicability and feasibility of SERS as a layer-by-layer interrogating tool. It is therefore suitable to distinguish the roles and location of different EPS components in the biofilm during biofouling and cleaning processes.

3.3.2 Cleaning after 48 h biofouling

On more severe 48-h biofouled membranes with aged biofilm, water flux was gradually recovered and reached 90.5% after 4 h cleaning (F-48/C-4; Fig. 6). The thickness of biofoulant in 48-h biofouled membrane (Fig. 7b) declined more rapidly than 18-h biofouled membrane (Fig. 7a), with most biofoulant being removed within the first 0.5 h and 1 h (F-48/C-0.5 and F-48/C-1). Accordingly, water flux recovery was also slightly improved (Fig. 6). Easier removal of sessile cells is associated with structural changes within severe 48-h biofouling. After 4-h cleaning, few bacteria were observed on the membrane surface, but water flux recovery could not achieve 100%. The persistence of residual biofilm substances on NF membrane surfaces after chemical cleaning would account for permanent permeability loss.

To demonstrate the changes occurred within 48-h biofouling, SERS spectra were acquired pre- and post-cleaning (Fig. 8c). Separated PCA-LDA clusters clearly illustrate the spectral alterations during cleaning (Fig. 8d). Most bands (Table 1) still display opposing intensity changes between biofouling and cleaning processes, similar to 18-h biofouling. Nevertheless, polysaccharide band at 494 cm^{-1} that appear in 48-h biofouling still persist on membranes after 0.5 h and 1 h cleaning, but are absent during cleaning of 18-h biofouled membrane. This suggests that a specific polysaccharide is exclusively formed after severe 48-h biofouling both on the surface and within the internal structure. Since the degradation of EPS by extracellular enzymes can promote detachment of bacteria from biofilms (Flemming and

Wingender, 2010, Park et al., 2012), the reformation of biofilm infrastructure accompanied with biochemical changes might explain the easier detachment of biofouling layer in cleaning severe 48-h biofouled membrane. In industrial cleaning processes, it was also found that sessile bacteria were removed from NF membranes but exopolysaccharides in a superficial layer of biofouling deposit were only partially eliminated (Di Martino et al., 2007). Therefore, our work provides deeper insights on how biofouling development and biochemical changes affect cleaning process.

3.4 *Relationship between biofouling compositions and cleaning efficiency*

To explore cleaning efficiency against different biofouling compositions and improve the procedure, relative intensities of SERS bands characteristic of DNA, lipid, polysaccharide and protein were calculated and compared during both processes at a closes normalized water flux. SERS bands employed were: 737 cm^{-1} (DNA), 1465 cm^{-1} (lipid), 494 cm^{-1} (polysaccharide) and 1000 cm^{-1} (protein). Relative intensities were calculated by dividing the integrated intensity of DNA, lipid and polysaccharide by that of protein. Normalized water flux in F-10, F-18/C-0.5 and F-48/C-0.5 (74.7%, 76.4% and 77.1%, respectively) was similar and approximately 76%, representing exponential biofouling development or insufficient cleaning. Meanwhile, the water flux in F-4, F-18/C-3 and F-48/C-4 (92.1%, 91.3% and 90.5%, respectively) was similar and approximately 91%, representing the initial bacterial attachment or the nearly sufficient cleaning.

In the 76% flux group, the relative intensity of polysaccharide in F-48/C-0.5 was the highest (Fig. 9), but that of lipid and DNA decreased post-cleaning in comparison with F-10, with greater decreases in lipid than DNA, especially in F-48/C-0.5. These results suggest that surfactant SDS is more efficient against lipid than DNA or polysaccharide. For the 91% flux group, the relative content of polysaccharides was

much lower, indicating their eventual removal after cleaning. The lipid formed after F-4 vanished post-cleaning, confirming again the good cleaning efficiency of SDS. The DNA content showed a relatively small decrease after cleaning, similar to 76% flux group, indicating a possibly moderate cleaning efficiency of SDS. Additionally, all of the relative contents in the 91% flux group were lower than those in the 76% flux group. This is due to the higher band intensity of protein in 91% flux recovery group despite of biofouling or cleaning process. Houari et al. (2010) also revealed a fouling substance-dependent cleaning efficiency in a NF membrane plant for drinking water production by applying commercial cleaning reagents, including alkaline, acids, metal chelating agents, surfactants and enzymes, which were more efficient against protein than polysaccharide. Alongside our work, this supports the idea of applying appropriate cleaning solutions to biofouling with different chemical compositions.

The residual substances on NF membranes that contributed to the permanent permeability loss were also investigated based on the spectra with a flux recovery ratio of more than 90% after chemical cleaning, *i.e.*, F-18/C-3 and F-48/C-4 (Fig. 8a, 8c). The dominant SERS bands observed were at 737 cm^{-1} (A of DNA), 1325 cm^{-1} (A, G of DNA), 1000 cm^{-1} (phenylalanine, protein), and 1630 cm^{-1} (Amide I, protein), were mainly from DNA and protein-related substances.

4. Conclusion

This work introduced SERS as a layer-by-layer interrogation tool to investigate the chemical variations of NF membrane biofouling during both formation and cleaning. The chemical compositions of biofouling, consisting of DNA, protein, lipid and polysaccharides, varied markedly and were associated with different biofouling stages induced by bacterial attachment, rapid growth, mature and aged biofilm. The

opposing changes of SERS bands during biofouling and cleaning processes indicate a layer-by-layer cleaning mode after short-term biofouling. In severe biofouling, *i.e.*, 48 h herein, biochemical changes were shown to occur on and within the biofilm, based on the exclusive appearance of polysaccharide band in SERS spectra. The easier detachment of 48-h biofouling indicated an alteration of biofilm infrastructure accompanying biochemical changes. Biofouling composition-dependent cleaning efficiency was evaluated with surfactant SDS acting most efficiently against lipid. Residual substances on NF membranes contributing to permanent permeability loss were identified as protein and DNA.

For the first time with the SERS layer-by-layer interrogation, some precise information on chemical variation, biochemical changes and cleaning efficiency is revealed. This work opens up the possibility of using SERS towards evaluating the efficiency of cleaning reagents and protocols. More practical attempts could involve applying SERS in industrial membrane processes and exploring the cleaning efficiency and mechanisms of different cleaning agents.

Acknowledgments This work was supported by the National Natural Science Foundation of China (21173208), Natural Science Foundation of Ningbo (2014A610107) and Fujian Province (2015J01067), China Scholarship Council, Youth Innovation Promotion Association of Chinese Academy of Sciences. *B. diminuta* was kindly provided by Prof. Xin Yu's laboratory in the Institute of Urban Environment, China.

Appendix A. Supplementary dada

Supplementary data related to this article can be found at

References

Al-Juboori, R.A. and Yusaf, T., 2012. Biofouling in RO system: mechanisms, monitoring and controlling. Desalination 302, 1-23.

Andrews, J.S., Rolfe, S.A., Huang, W.E., Scholes, J.D. and Banwart, S.A., 2010. Biofilm formation in environmental bacteria is influenced by different macromolecules depending on genus and species. Environ. Microbiol. 12(9), 2496-2507.

Baek, Y., Yu, J., Kim, S.H., Lee, S. and Yoon, J., 2011. Effect of surface properties of reverse osmosis membranes on biofouling occurrence under filtration conditions. J. Membr. Sci. 382(1-2), 91-99.

Bes-Pia, A., Cuartas-Uribe, B., Mendoza-Roca, J.A. and Alcaina-Miranda, M.I., 2010. Study of the behaviour of different NF membranes for the reclamation of a secondary textile effluent in rinsing processes. J. Hazard. Mater. 178(1-3), 341-348.

Chao, Y.Q. and Zhang, T., 2012. Surface-enhanced Raman scattering (SERS) revealing chemical variation during biofilm formation: from initial attachment to mature biofilm. Anal. Bioanal. Chem 404(5), 1465-1475.

Chen, P.Y., Cui, L. and Zhang, K.S., 2015. Surface-enhanced Raman spectroscopy monitoring the development of dual-species biofouling on membrane surfaces. J. Membr. Sci. 473, 36–44.

Cui, L., Chen, P.Y., Chen, S.D., Yuan, Z.H., Yu, C.P., Ren, B. and Zhang, K.S., 2013. In situ study of the antibacterial activity and mechanism of action of silver nanoparticles by surface-enhanced Raman spectroscopy. Anal. Chem. 85(11), 5436-5443.

Cui, L., Chen, S.D. and Zhang, K.S., 2015. Effect of toxicity of Ag nanoparticles on SERS spectral variance of bacteria. Spectroc. Acta Pt. A-Molec. Biomolec. Spectr. 137(0), 1061-1066.

Cui, L., Yao, M., Ren, B. and Zhang, K.-S., 2011. Sensitive and Versatile Detection of the Fouling Process and Fouling Propensity of Proteins on Polyvinylidene

534 Fluoride Membranes via Surface-Enhanced Raman Spectroscopy. Anal. Chem.
535 83(5), 1709-1716.
536 Di Martino, P., Doumeche, B., Galas, L., Vaudry, H., Heim, V. and Habarou, H., 2007.
537 Assessing chemical cleaning of nanofiltration membranes in a drinking water
538 production plant: a combination of chemical composition analysis and
539 fluorescence microscopy. Water Sci. Technol. 55(8-9), 219-225.
540 Flemming, H.C., 2002. Biofouling in water systems - cases, causes and
541 countermeasures. Appl. Microbiol. Biotechnol. 59(6), 629-640.
542 Flemming, H.C., Schaule, G., Griebe, T., Schmitt, J. and Tamachkiarowa, A., 1997.
543 Biofouling - the Achilles heel of membrane processes. Desalination 113(2-3),
544 215-225.
545 Flemming, H.C. and Wingender, J., 2010. The biofilm matrix. Nat. Rev. Microbiol.
546 8(9), 623-633.
547 Frens, G., 1973. Controlled nucleation for regulation of particle-size in monodisperse
548 gold suspensions. Nature-Phys Sci 241(105), 20-22.
549 Gonder, Z.B., Arayici, S. and Barles, H., 2011. Advanced treatment of pulp and paper
550 mill wastewater by nanofiltration process: Effects of operating conditions on
551 membrane fouling. Sep. Purif. Technol. 76(3), 292-302.
552 Guo, W., Ngo, H.-H. and Li, J., 2012. A mini-review on membrane fouling. Bioresour.
553 Technol. 122, 27-34.
554 Herzberg, M. and Elimelech, M., 2007. Biofouling of reverse osmosis membranes:
555 Role of biofilm-enhanced osmotic pressure. J. Membr. Sci. 295(1-2), 11-20.
556 Herzberg, M., Kang, S. and Elimelech, M., 2009. Role of extracellular polymeric
557 substances (EPS) in biofouling of reverse osmosis membranes. Environ. Sci.
558 Technol. 43(12), 4393-4398.
559 Houari, A., Habarou, H., Djafer, M., Heim, V. and Di Martino, P., 2009. Effect of
560 storage of NF membranes on fouling deposits and cleaning efficiency. Desalin
561 Water Treat 1(1-3), 307-311.
562 Houari, A., Seyer, D., Couquard, F., Kecili, K., Democrate, C., Heim, V. and Di
563 Martino, P., 2010. Characterization of the biofouling and cleaning efficiency

564 of nanofiltration membranes. Biofouling 26(1), 15-21.
565 Huang, H., Young, T. and Jacangelo, J.G., 2009a. Novel approach for the analysis of
566 bench-scale, low pressure membrane fouling in water treatment. J. Membr. Sci.
567 334(1-2), 1-8.
568 Huang, W.E., Ward, A.D. and Whiteley, A.S., 2009b. Raman tweezers sorting of
569 single microbial cells. Environ. Microbiol. Rep. 1(1), 44-49.
570 Ivleva, N.P., Wagner, M., Horn, H., Niessner, R. and Haisch, C., 2009. Towards a
571 nondestructive chemical characterization of biofilm matrix by Raman
572 microscopy. Anal. Bioanal. Chem 393, 197-206.
573 Ivleva, N.P., Wagner, M., Szkola, A., Horn, H., Niessner, R. and Haisch, C., 2010.
574 Label-free in situ SERS imaging of biofilms. J. Phys. Chem. B 114(31),
575 10184-10194.
576 Judd, S. and Jefferson, B., 2003. Membranes for Industrial Wastewater Recovery and
577 Re-use, Elsevier Science Ltd., Oxford, UK.
578 Kneipp, J., Kneipp, H. and Kneipp, K., 2008. SERS - a single-molecule and nanoscale
579 tool for bioanalytics. Chem. Soc. Rev. 37(5), 1052-1060.
580 Kneipp, K., Haka, A.S., Kneipp, H., Badizadegan, K., Yoshizawa, N., Boone, C.,
581 Shafer-Peltier, K.E., Motz, J.T., Dasari, R.R. and Feld, M.S., 2002.
582 Surface-enhanced Raman Spectroscopy in single living cells using gold
583 nanoparticles. Appl. Spectrosc. 56(2), 150-154.
584 Kwon, S., Moon, E., Kim, T.S., Hong, S. and Park, H.D., 2011. Pyrosequencing
585 Demonstrated Complex Microbial Communities in a Membrane Filtration
586 System for a Drinking Water Treatment Plant. Microbes Environ 26(2),
587 149-155.
588 Li, Q.L. and Elimelech, M., 2004. Organic fouling and chemical cleaning of
589 nanofiltration membranes: Measurements and mechanisms. Environ. Sci.
590 Technol. 38(17), 4683-4693.
591 Liikanen, R., Yli-Kuivila, J. and Laukkanen, R., 2002. Efficiency of various chemical
592 cleanings for nanofiltration membrane fouled by conventionally-treated
593 surface water. J. Membr. Sci. 195(2), 265-276.

Liu, Y., Liu, H.N., Cui, L. and Zhang, K.S., 2012. The ratio of food-to-microorganism (F/M) on membrane fouling of anaerobic membrane bioreactors treating low-strength wastewater. Desalination 297, 97-103.

Maquelin, K., Kirschner, C., Choo-Smith, L.P., van den Braak, N., Endtz, H.P., Naumann, D. and Puppels, G.J., 2002. Identification of medically relevant microorganisms by vibrational spectroscopy. J. Microbiol. Methods 51(3), 255-271.

Martin, F.L., Kelly, J.G., Llabjani, V., Martin-Hirsch, P.L., Patel, I.I., Trevisan, J., Fullwood, N.J. and Walsh, M.J., 2010. Distinguishing cell types or populations based on the computational analysis of their infrared spectra. Nat. Protoc. 5(11), 1748-1760.

Mendret, J., Guigui, C., Schmitz, R. and Cabassud, C., 2009. In situ dynamic characterisation of fouling under different pressure conditions during dead-end filtration: Compressibility properties of particle cakes. J. Membr. Sci. 333(1-2), 20-29.

Nguyen, T., Roddick, F.A. and Fan, L., 2012. Biofouling of water treatment membranes: a review of the underlying causes, monitoring techniques and control measures. Membranes 2, 804-840.

Ortiz, A., Teruel, J.A., Espuny, M.J., Marques, A., Manresa, A. and Aranda, F.J., 2009. Interactions of a bacterial biosurfactant trehalose lipid with phosphatidylserine membranes. Chem. Phys. Lipids 158(1), 46-53.

Park, J.H., Lee, J.H., Cho, M.H., Herzberg, M. and Lee, J., 2012. Acceleration of protease effect on Staphylococcus aureus biofilm dispersal. FEMS Microbiol. Lett. 335(1), 31-38.

Pirog, T.P., Shevchuk, T.A., Voloshina, I.N. and Karpenko, E.V., 2004. Production of surfactants by Rhodococcus erythropolis strain EK-1, grown on hydrophilic and hydrophobic substrates. Appl. Biochem. Microbiol. 40(5), 470-475.

Rosch, P., Harz, M., Schmitt, M., Peschke, K.D., Ronneberger, O., Burkhardt, H., Motzkus, H.W., Lankers, M., Hofer, S., Thiele, H. and Popp, J., 2005. Chemotaxonomic identification of single bacteria by micro-Raman

624 spectroscopy: Application to clean-room-relevant biological contaminations.
625 Appl. Environ. Microbiol. 71(3), 1626-1637.
626 Sandt, C., Smith-Palmer, T., Pink, J., Brennan, L. and Pink, D., 2007. Confocal
627 Raman microspectroscopy as a tool for studying the chemical heterogeneities
628 of biofilms in situ. J. Appl. Microbiol. 103(5), 1808-1820.
629 Sim, S.T.V., Suwarno, S.R., Chong, T.H., Krantz, W.B. and Fane, A.G., 2013.
630 Monitoring membrane biofouling via ultrasonic time-domain reflectometry
631 enhanced by silica dosing. J. Membr. Sci. 428, 24-37.
632 Talari, A.C.S., Movasaghi, Z., Rehman, S. and Rehman, I.U., 2014. Raman
633 spectroscopy of biological tissues. Appl. Spectrosc. Rev. 50(1), 46-111.
634 Tung, K.L., Damodar, H.R., Damodar, R.A., Wu, T.T., Li, Y.L., Lin, N.J., Chuang,
635 C.J., You, S.J. and Hwang, K.J., 2012. Online monitoring of particle fouling in
636 a submerged membrane filtration system using a photointerrupt sensor array. J.
637 Membr. Sci. 407, 58-70.
638 Wagner, M., Ivleva, N.P., Haisch, C., Niessner, R. and Horn, H., 2009. Combined use
639 of confocal laser scanning microscopy (CLSM) and Raman microscopy (RM):
640 Investigations on EPS - Matrix. Water Res. 43(1), 63-76.
641 Xu, L.J., Zong, C., Zheng, X.S., Hu, P., Feng, J.M. and Ren, B., 2014. Label-free
642 detection of native proteins by surface-enhanced Raman spectroscopy using
643 iodide-modified nanoparticles. Anal. Chem. 86(4), 2238-2245.
644 Yao, M., Zhang, K. and Cui, L., 2010. Characterization of protein-polysaccharide
645 ratios on membrane fouling. Desalination 259(1-3), 11-16.
646 Yuan, B., Wang, X., Tang, C., Li, X. and Yu, G., 2015. In situ observation of the
647 growth of biofouling layer in osmotic membrane bioreactors by multiple
648 fluorescence labeling and confocal laser scanning microscopy. Water Res. 75,
649 188-200.
650 Zhang, J., Loong, W.L.C., Chou, S., Tang, C., Wang, R. and Fane, A.G., 2012a.
651 Membrane biofouling and scaling in forward osmosis membrane bioreactor. J.
652 Membr. Sci. 403, 8-14.
653 Zhang, M.Y., Zhang, K.S., De Gusseme, B. and Verstraete, W., 2012b. Biogenic silver

nanoparticles (bio-Ag-0) decrease biofouling of bio-Ag-0/PES nanocomposite membranes. Water Res. 46(7), 2077-2087.

Figure captions

Fig. 1 – Schematic of laboratory-scale crossflow NF membrane filtration system.

Fig. 2 – Normalized flux decline curve upon induced biofouling with synthetic wastewater medium inoculated with *B. diminuta* in five cascade-connected biofouling experiments terminated at 4 h, 10 h, 14 h, 26 h, 48 h. Experimental conditions: initial permeate flux of pure water of 41 $L/m^2/h$, crossflow velocity of 8 cm/s, initial cell concentration of 10^6 CFU/mL, pressure of 0.5 MPa.

Fig. 3 – Surface and cross-sectional view of SEM images of NF membranes biofouled by synthetic wastewater inoculated with *B. diminuta* after filtration time in the images.

Fig. 4 – SEM images of Au NPs covered on biofouled membrane.

Fig. 5 – SERS spectra (a) and PCA-LDA scores plot (b) of biofouled membrane terminated at 4 h, 10 h, 14 h, 26 h and 48 h, respectively. Corona around the mean SERS spectra indicates standard deviation of numerous spectra acquired from one biofouled membrane.

Fig. 6 – Water flux recovery ratio of 18-h (F-18, blue) and 48-h (F-48, red) biofouled membrane cleaned by 0.025% SDS and NaOH (pH 12) for 0.5 h, 1 h, 3 h or 4 h. Cleaning was performed at 0 MPa (no permeation) and a crossflow velocity of 48 cm/s. The ratio was calculated by dividing the water flux of NF membrane after cleaning by that before biofouling.

Fig. 7 – Surface and cross-sectional view of SEM images of 18-h (a) and 48-h biofouled (b) membrane pre- and post-cleaning for 0.5 h, 1 h, 3 h or 4 h.

682 **Fig. 8 –** SERS spectra (a, c) and PCA-LDA scores plots (b, d) of 18 h (a, b) and 48
683 h-biofouled (c, d) membranes pre- and post-cleaning for 0.5 h, 1 h, 3 h or 4 h. Corona
684 around the SERS spectra indicate the standard deviation of numerous spectra acquired
685 from one biofouled membrane.

686 **Fig. 9 –** Integrated Raman intensity ratio of Polysaccharide/Protein (494/1000),
687 Lipid/Protein (1465/1000), DNA/Protein (737/1000) during biofouling and cleaning
688 at two normalized water fluxes around 76% and 91%.

689

690 **Table 1.** Variations and assignments of SERS bands of membrane biofouling during
691 formation and two cleaning processes (Andrews et al., 2010, Cui et al., 2013, Ivleva et
692 al., 2010, Talari et al., 2014). Red or blue arrows represent increases or decreases in
693 respective Raman intensity during biofouling and cleaning processes.

694

Origin	**Band (cm^{-1})**	**Formation**	**Cleaning after 18 h biofouling**	**Cleaning after 48 h biofouling**	**Tentative band Assignments**
Carbohydrate	494	↑	/	↑	Skeletal mode CC, CCC ring deformation
	550	↑	/	↓	C-O glycosidic ring deformation
	1095	↑	↓	↓	C-C str, C-O-C glycosidic link
	1126	↑	↓	↓	C-C str, C-O-C glycosidic link
DNA	660	↑	↓	↓	Ring breathing of G
	737	↑	↓	↓	Ring breathing of A
	1325	↑	↓	↓	Adenosine
	1587	↓↑	↑↓	↓	Ring stretching of Guanosine
Protein	1000	↓	↑	↑	Ring breathing of Phenylalanine
	1243	↑	↓	↓	Amide III
	1700	↑	↓	↓	Amide I
	1445	↓	↑	↑	CH_2 deformation
Lipid	1465	↑	↓	↓	CH_2 deformation
Carotenoids	1533	↓	↑	↑	C=C stretching

695

Figure

Fig. 1

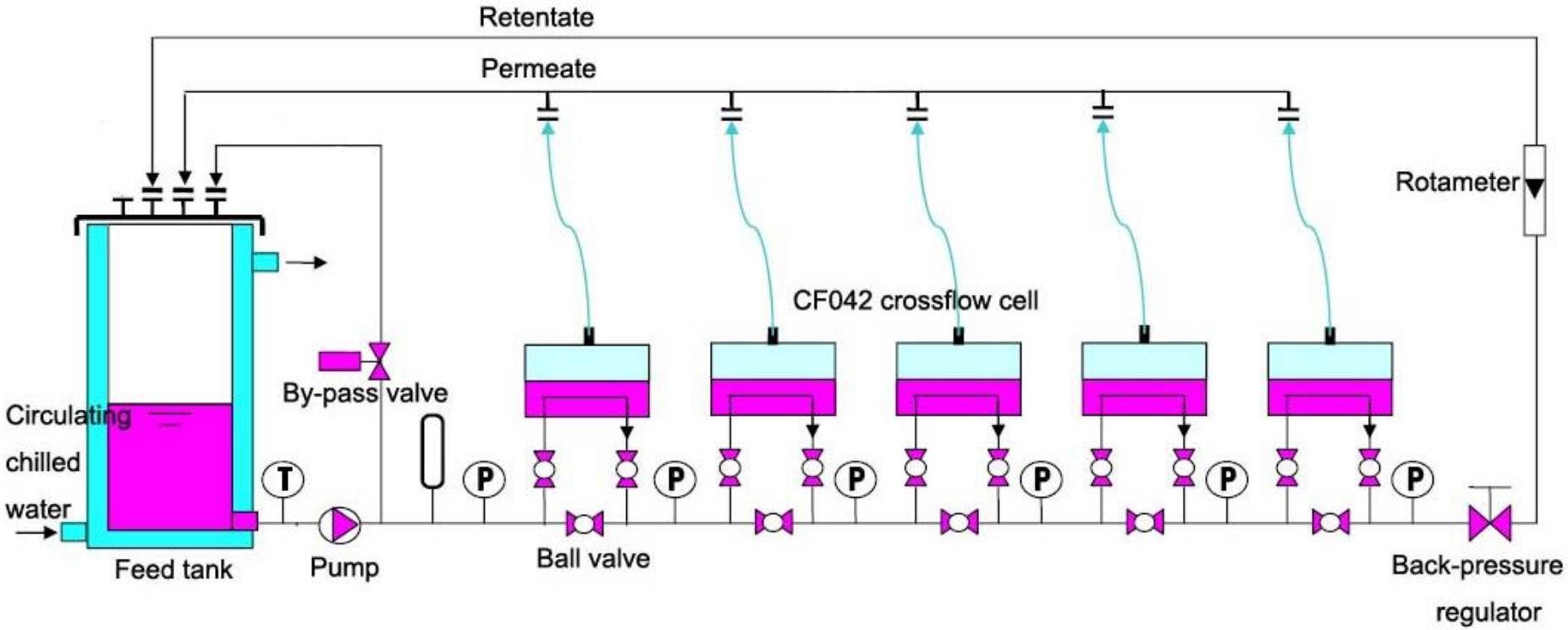
Retentate
Permeate
Rotameter
CF042 crossflow cell
By-pass valve
Circulating
chilled
water
T
P
Feed tank
Pump
Ball valve
Back-pressure
regulator

Fig. 2

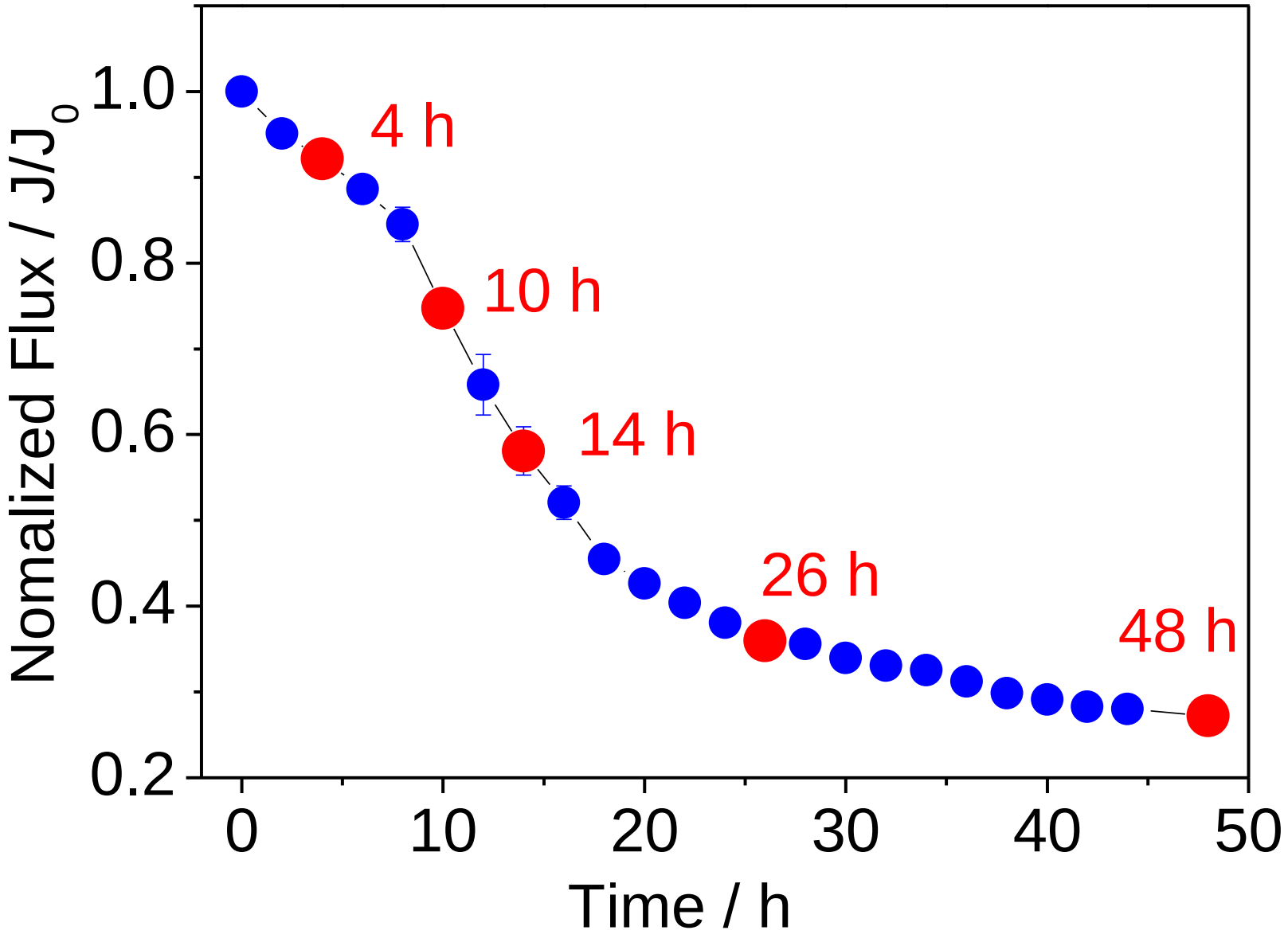
Nomalized Flux / J/J0
1.0
0.8
0.6
0.4
0.2
0
10
20
30
40
50
Time / h
4 h
10 h
14 h
26 h
48 h

Fig. 3

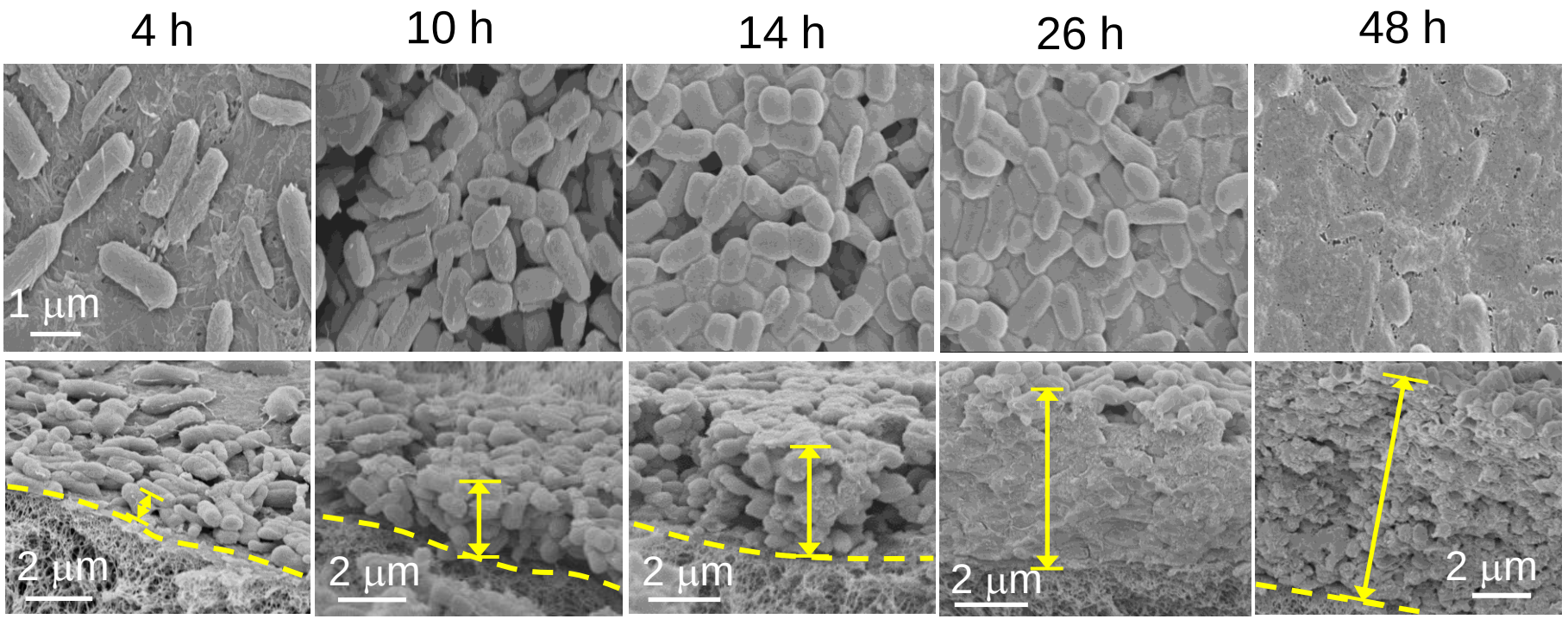

Fig. 4

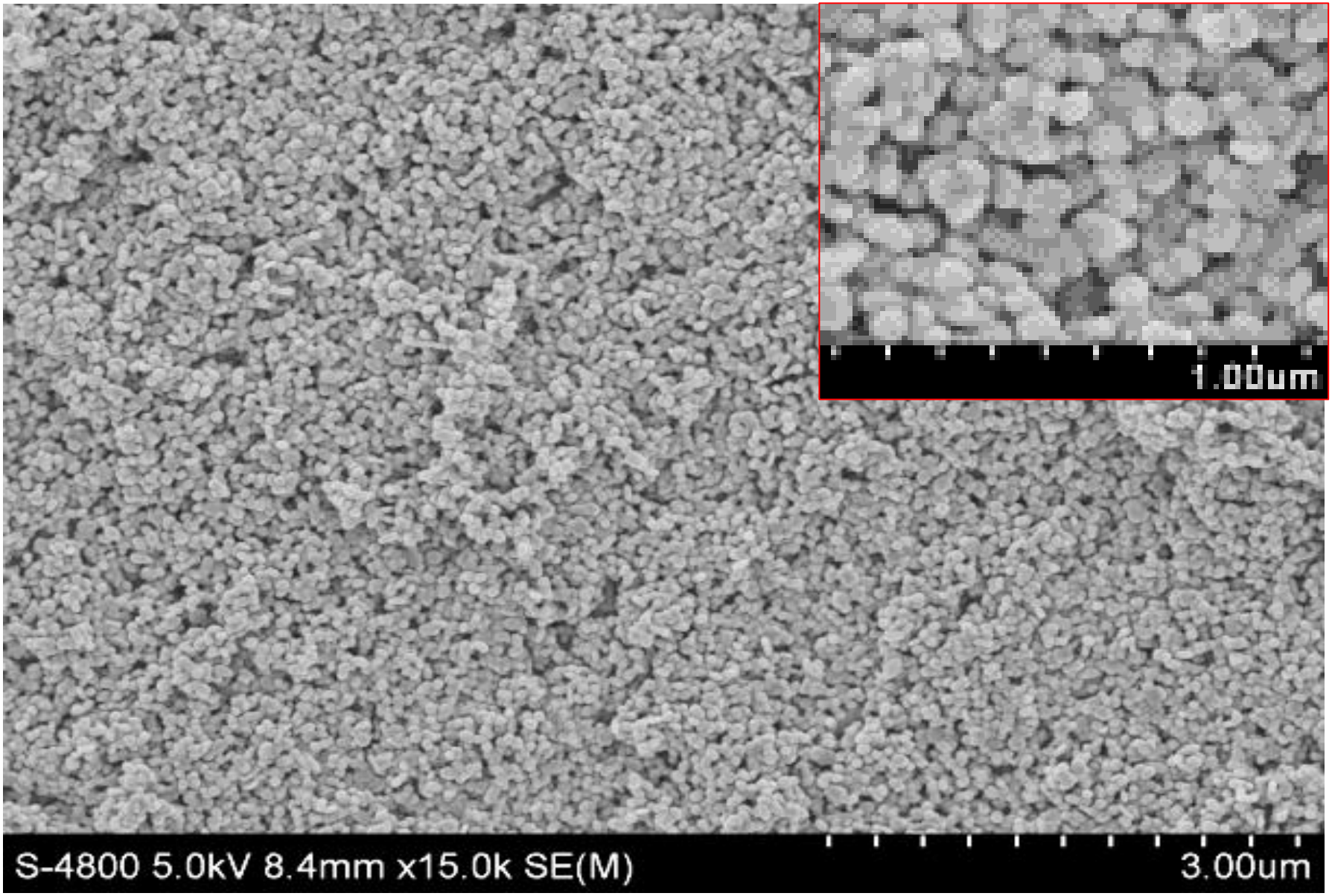

Fig. 5

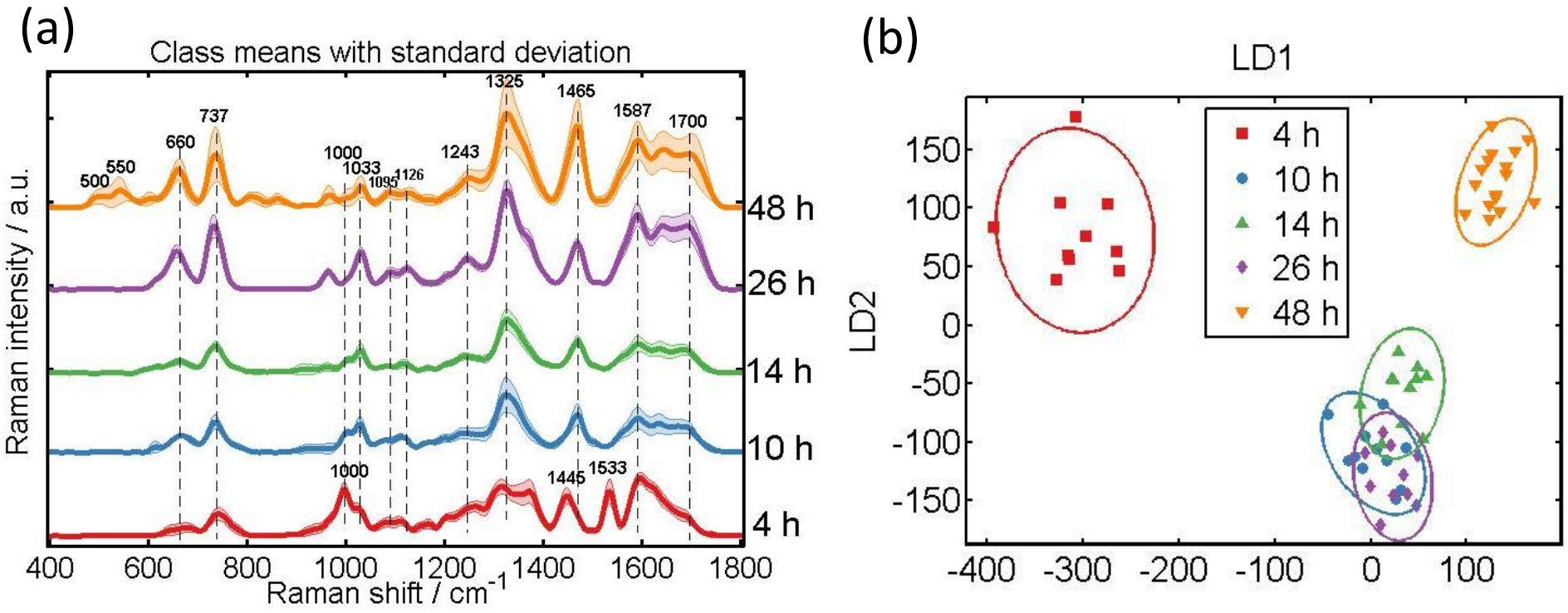
(a)
Class means with standard deviation
Raman intensity / a.u.
Raman shift / cm-1
500
550
660
737
1000
1033
1095
1126
1243
1325
1465
1587
1700
48 h
26 h
14 h
10 h
4 h
1000
1445
1533
400
600
800
1000
1200
1400
1600
1800
(b)
LD1
LD2
4 h
10 h
14 h
26 h
48 h
150
100
50
0
-50
-100
-150
-400
-300
-200
-100
0
100

Fig. 6

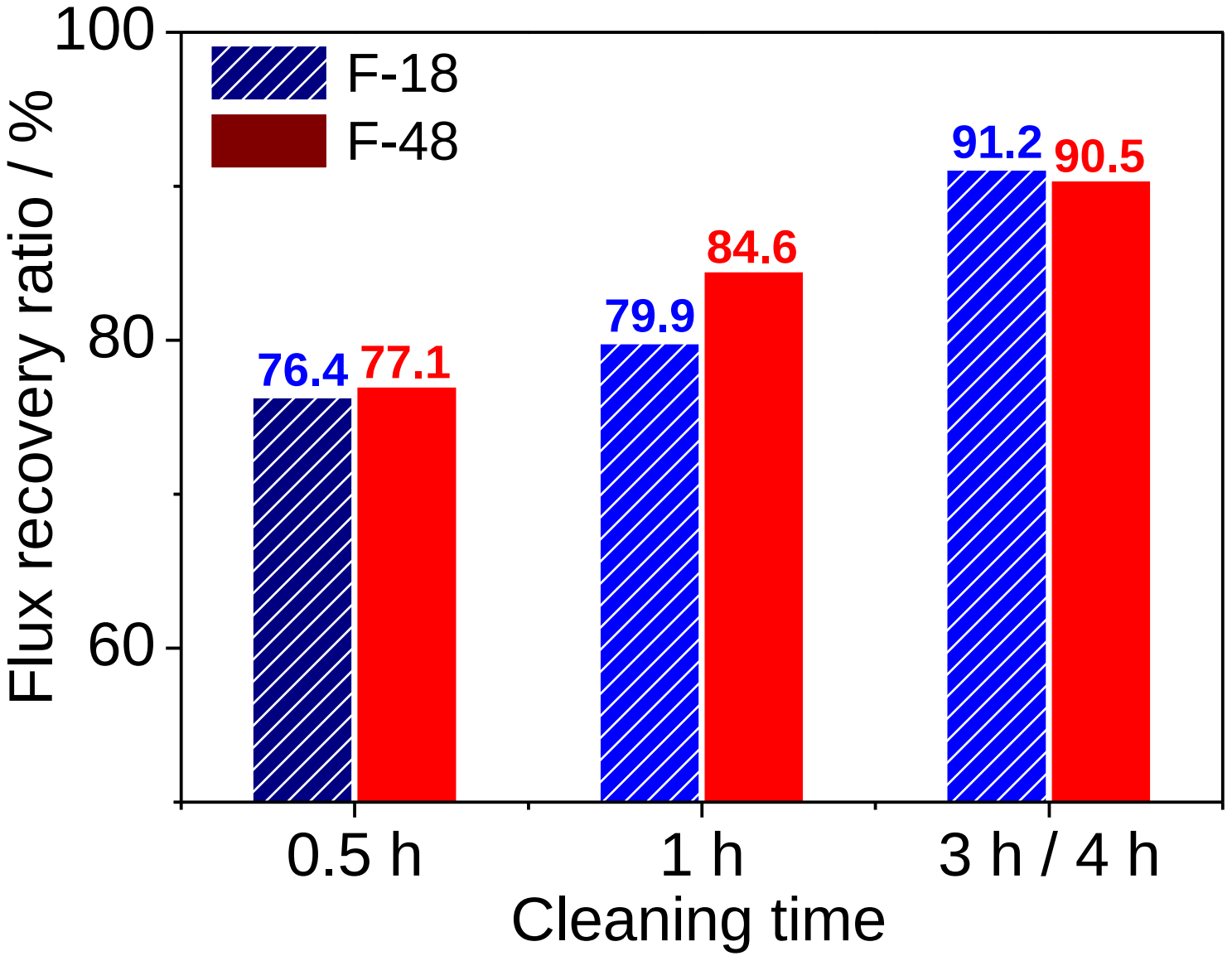
100
80
60
Flux recovery ratio / %
F-18
F-48
76.4
77.1
79.9
84.6
91.2
90.5
0.5 h
1 h
3 h / 4 h
Cleaning time

Fig. 7

(a)

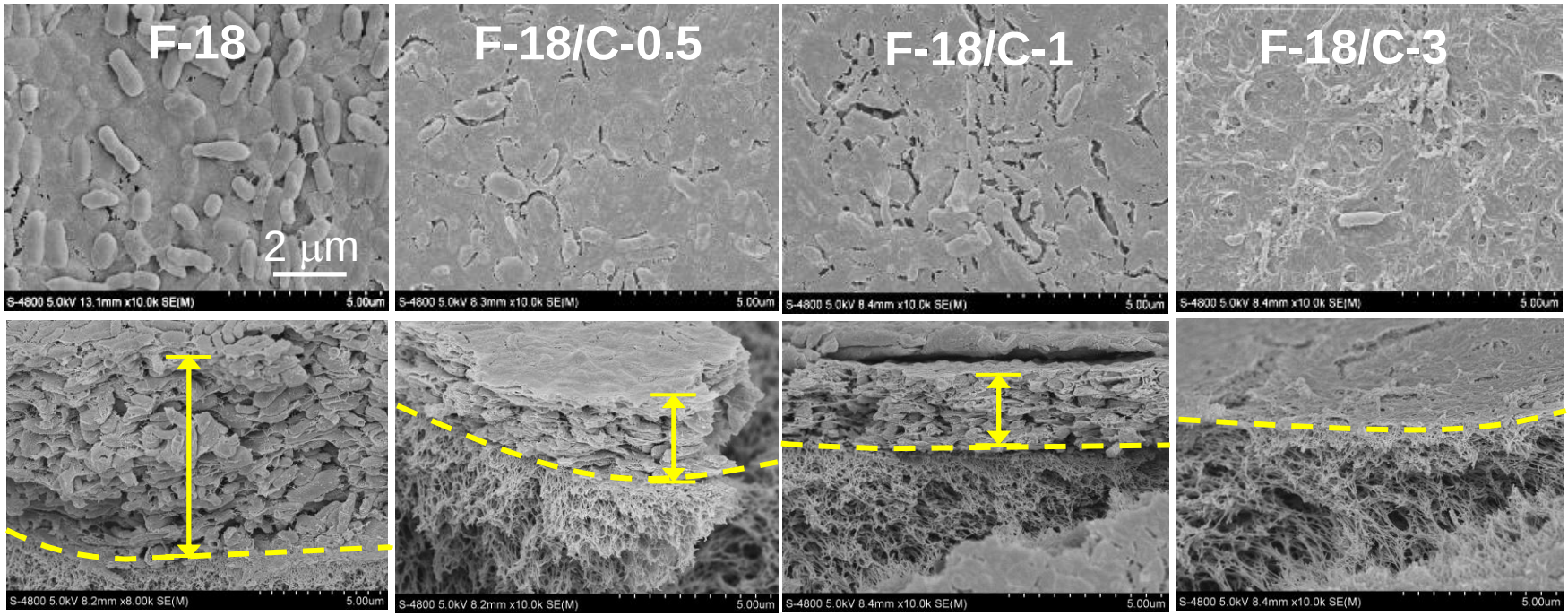
F-18
F-18/C-0.5
F-18/C-1
F-18/C-3
2 μm
S-4800 5.0kV 13.1mm x10.0k SE(M)
S-4800 5.0kV 8.3mm x10.0k SE(M)
S-4800 5.0kV 8.4mm x10.0k SE(M)
S-4800 5.0kV 8.4mm x10.0k SE(M)
S-4800 5.0kV 8.2mm x8.00k SE(M)
S-4800 5.0kV 8.2mm x10.0k SE(M)
S-4800 5.0kV 8.4mm x10.0k SE(M)
S-4800 5.0kV 8.4mm x10.0k SE(M)
5.00um

(b)

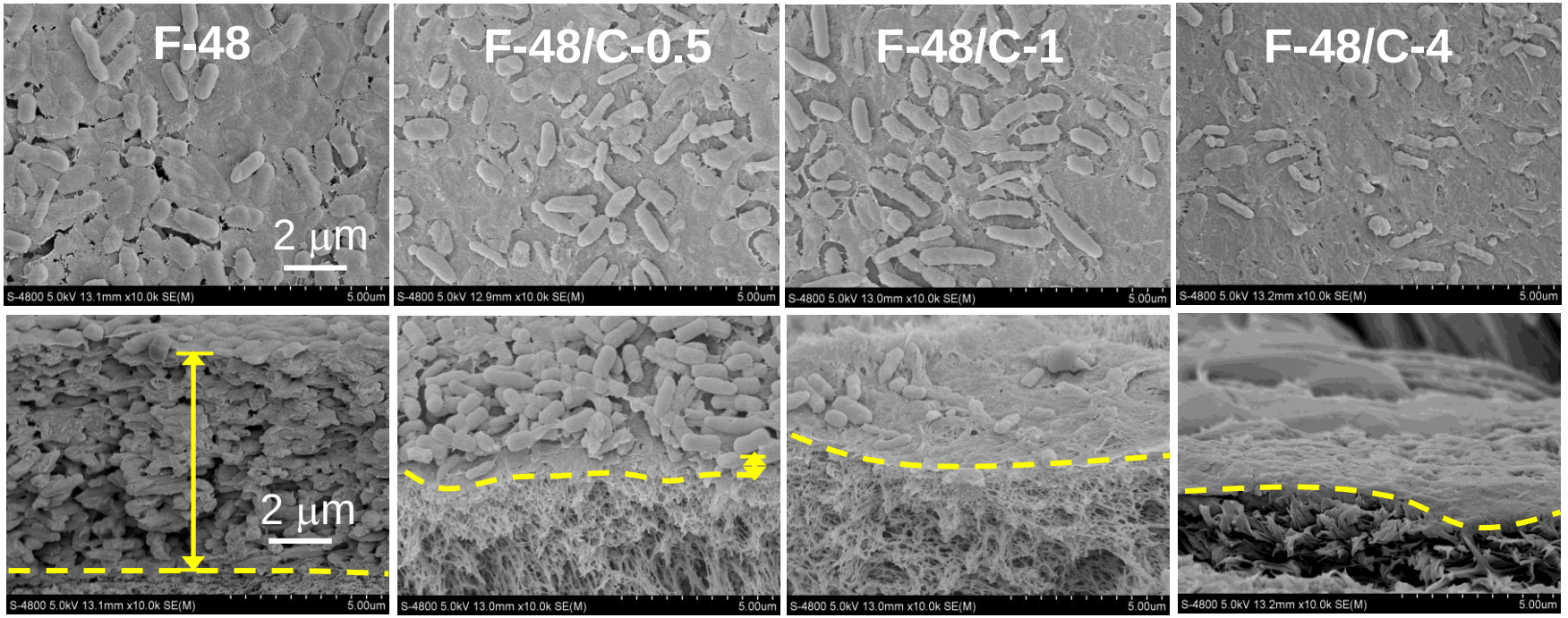
F-48
F-48/C-0.5
F-48/C-1
F-48/C-4
2 μm
S-4800 5.0kV 13.1mm x10.0k SE(M)
S-4800 5.0kV 12.9mm x10.0k SE(M)
S-4800 5.0kV 13.0mm x10.0k SE(M)
S-4800 5.0kV 13.2mm x10.0k SE(M)
S-4800 5.0kV 13.1mm x10.0k SE(M)
S-4800 5.0kV 13.0mm x10.0k SE(M)
S-4800 5.0kV 13.0mm x10.0k SE(M)
S-4800 5.0kV 13.2mm x10.0k SE(M)
5.00um

Fig. 8

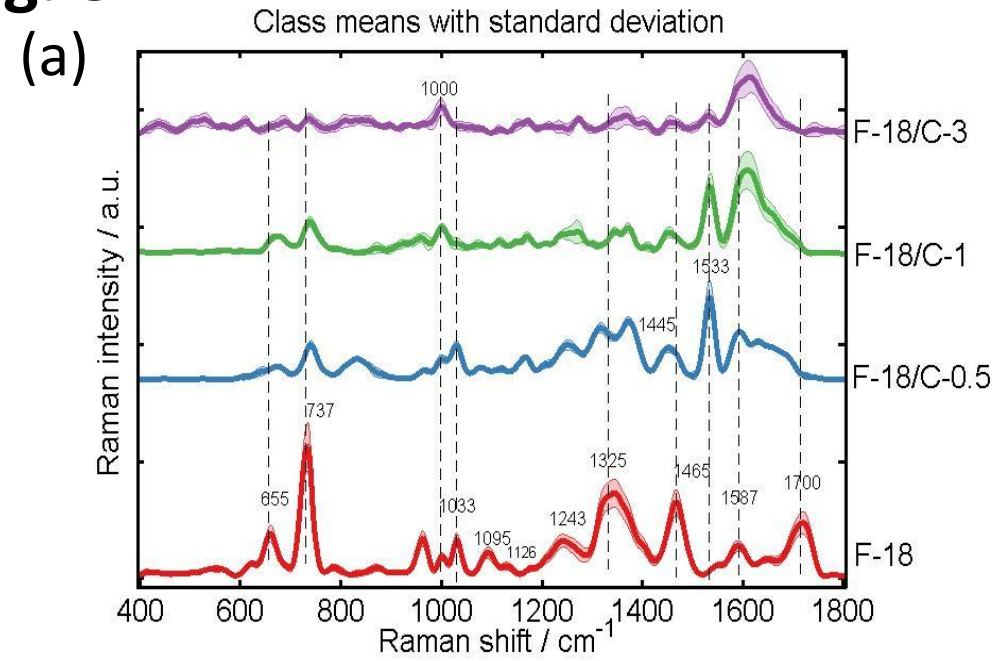
(a)
Class means with standard deviation
Raman intensity / a.u.
Raman shift / cm-1
F-18/C-3
F-18/C-1
F-18/C-0.5
F-18
1000
1533
1445
737
655
1325
1465
1587
1700
1033
1095
1126
1243
400
600
800
1000
1200
1400
1600
1800

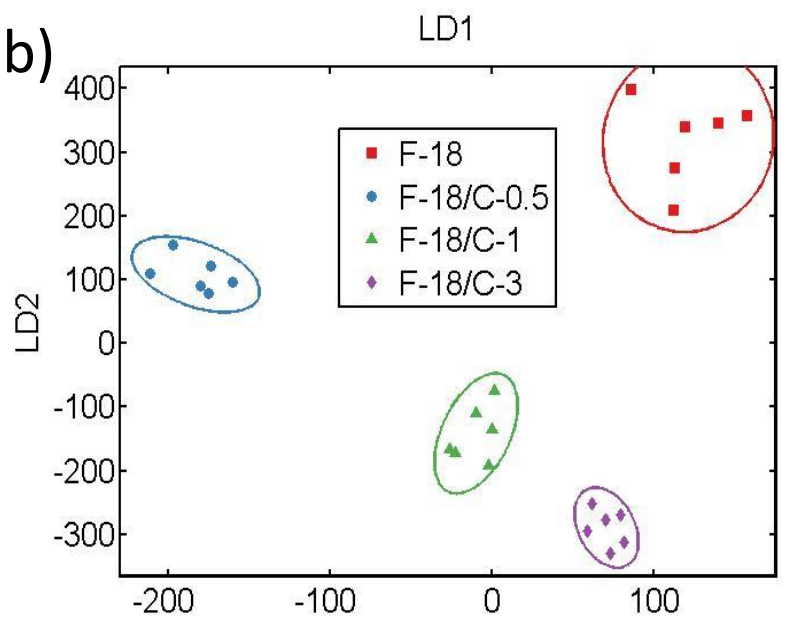
(b)
LD1
LD2
F-18
F-18/C-0.5
F-18/C-1
F-18/C-3
400
300
200
100
0
-100
-200
-300
-200
-100
0
100

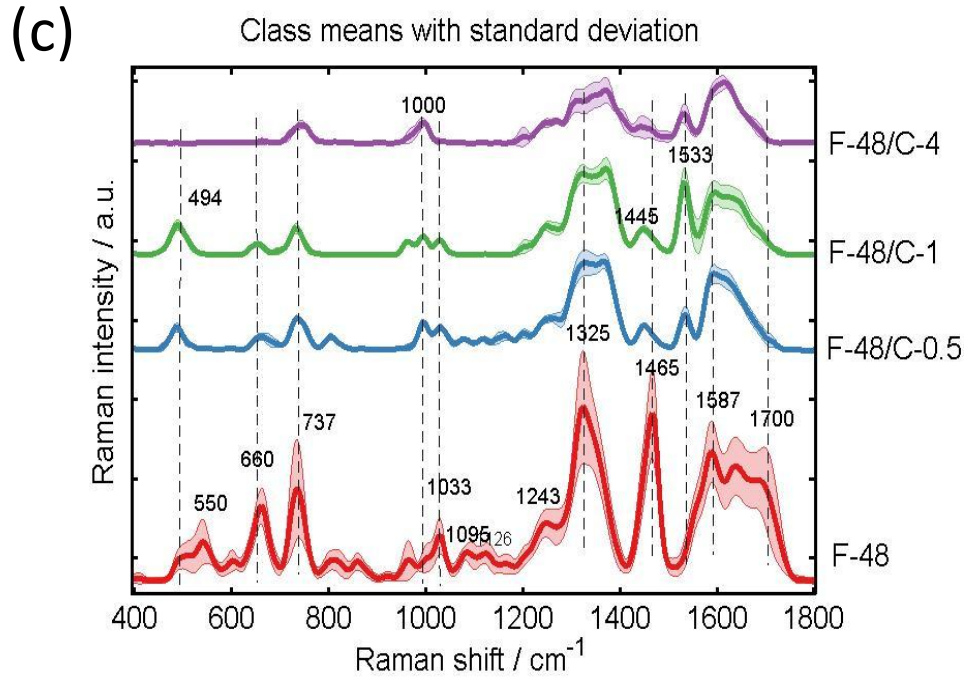
(c)
Class means with standard deviation
Raman intensity / a.u.
Raman shift / cm-1
F-48/C-4
F-48/C-1
F-48/C-0.5
F-48
1000
1533
494
1445
1325
1465
1587
1700
737
660
550
1033
1095
1243
400
600
800
1000
1200
1400
1600
1800

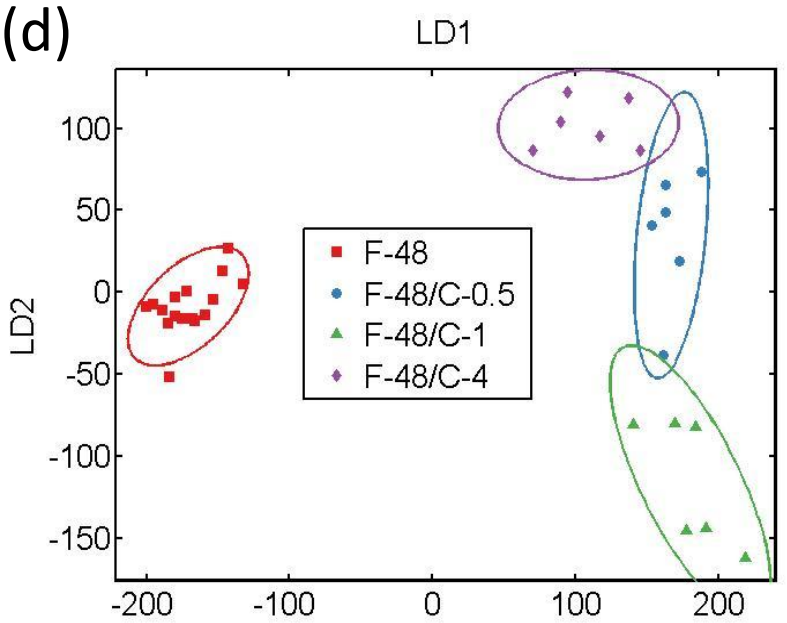
(d)
LD1
LD2
F-48
F-48/C-0.5
F-48/C-1
F-48/C-4
100
50
0
-50
-100
-150
-200
-100
0
100
200

Fig. 9

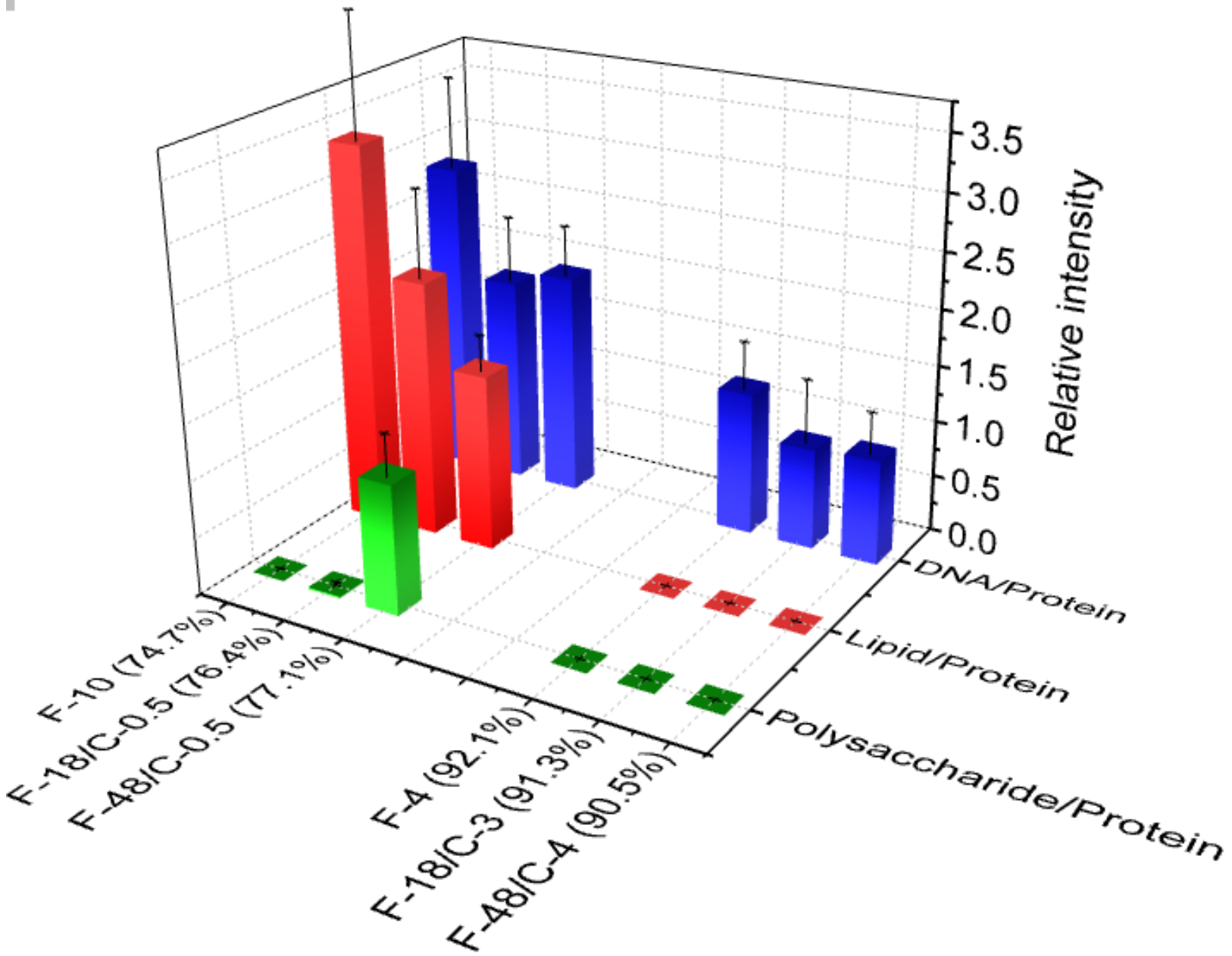
Relative intensity
3.5
3.0
2.5
2.0
1.5
1.0
0.5
0.0
DNA/Protein
Lipid/Protein
Polysaccharide/Protein
F-10 (74.7%)
F-18/C-0.5 (76.4%)
F-48/C-0.5 (77.1%)
F-4 (92.1%)
F-18/C-3 (91.3%)
F-48/C-4 (90.5%)

Electronic Supplementary Material (for online publication only)

Click here to download Electronic Supplementary Material (for online publication only): SI.docx